A Self-Quenched Galactosamine-Serum Albumin-RhodamineX Conjugate: A "Smart" Fluorescent Molecular Imaging Probe Synthesized with Clinically Applicable Material for Detecting Peritoneal Ovarian Cancer Metastases

Yukihiro Hama,[1] Yasuteru Urano,[2] Yoshinori Koyama,[1] Andrew J. Gunn,[1] Peter L. Choyke,[1] and Hisataka Kobayashi[1]

Abstract

Purpose: Fluorophore activation after cellular internalization of a targeted fluorescently labeled conjugate is an effective molecular imaging strategy to increase target-to-background ratios. The D-galactose receptor on ovarian cancer cells has been used to target self-quenched avidin-rhodamineX conjugates in which the avidin component binds to D-galactose receptor and the rhodamines are optically activated by dequenching only after cellular internalization. As a non-immunogenic alternative of avidin, galactosamine-conjugated serum albumin (GmSA) targets the D-galactose receptor with higher binding affinity and has more conjugation sites available for rhodamineX than avidin.

Experimental Design: GmSA was conjugated with 20 rhodamineX molecules (GmSA-20ROX) to create a self-quenching complex, which was compared with a conjugate consisting of GmSA and a single rhodamineX (GmSA-1ROX) in *ex vivo* chemical activation characteristics, intracellular activation, and *in vivo* molecular imaging for detecting peritoneal micrometastases of SHIN3 ovarian cancer.

Results: GmSA-20ROX was five times brighter than GmSA-1ROX when incubated with SHIN3 ovarian cancer cells for 3 h. Submillimeter SHIN3 ovarian cancer implants in the peritoneal cavity were clearly visualized *in vivo* with spectral fluorescence imaging due to the high tumor-to-background ratio. The sensitivity and specificity of GmSA-20ROX for implant detection were determined by colocalization of the rhodamineX emission with red fluorescent protein expressed constitutively in the SHIN3 tumor implants. Among 336 lesions, sensitivity and specificity were 99%/99%, respectively, for GmSA-20ROX, whereas the results for GmSA-1ROX were only 24%/100% ($n = 388$), respectively, for lesions ~0.8 mm or greater in diameter.

Conclusion: Self-quenched GmSA-20ROX is more efficient than previous D-galactose–targeted fluorescent conjugates.

Improving the detection of ovarian cancer peritoneal metastases during surgical resection could lead to better cancer outcomes. Optical fluorescence imaging has been proposed as means of guiding surgical resections because of its high sensitivity, its low cost, its compatibility with the operating room environment, and its absence of ionizing radiation (1). Several approaches have been proposed for enhancing the detection of cancer foci, including somatostatin receptor-targeted probes (2), folate receptor-targeted agents (3), D-galactose (asialo) receptor-targeted agents (1, 4–8), tumor-associated protease activatable agents (9–11), and hybrid viral particles (12). To achieve high sensitivity, the signal from the target tissue must greatly surpass the signal from the background and the extent to which the target-to-background ratio is maximized determines the ultimate sensitivity of the complex.

A common approach to optimize target-to-background ratios is to use fluorophore activation wherein the fluorophore emits minimal light in the unactivated state but increases its emission several fold in the activated state. For instance, Weissleder et al. have developed a series of agents activated by tumor-associated proteases [e.g., cathepsin D and matrix metalloproteinase-2 (MMP-2)], which function to dequench the complex resulting in a multifold increase in fluorescence (9–11). As an alternative, a self-quenching avidin-3 rhodamineX probe was synthesized, which binds D-galactose receptor on cancer cells and then is internalized (5). Intracellular

Authors' Affiliations: [1]Molecular Imaging Program, Center for Cancer Research, National Cancer Institute, NIH, Bethesda, Maryland and [2]Graduate School of Pharmaceutical Sciences, The University of Tokyo, Tokyo, Japan

Received 4/27/07; revised 7/13/07; accepted 8/2/07.

Grant support: Intramural Research Program of the NIH, National Cancer Institute, Center for Cancer Research.

The costs of publication of this article were defrayed in part by the payment of page charges. This article must therefore be hereby marked *advertisement* in accordance with 18 U.S.C. Section 1734 solely to indicate this fact.

Note: Supplementary data for this article are available at Clinical Cancer Research Online (http://clincancerres.aacrjournals.org/).

Requests for reprints: Hisataka Kobayashi, Molecular Imaging Program, Center for Cancer Research, National Cancer Institute/NIH, Building 10, Room 1B40, MSC 1088, 10 Center Drive, Bethesda, MD 20892-1088. Phone: 301-435-4086; Fax: 301-402-3191; E-mail: Kobayash@mail.nih.gov.

doi:10.1158/1078-0432.CCR-07-1004

endosomal or lysosomal dissociation of the avidin-3 rhodamineX complex leads to "dequenching" of the 3 rhodamineX molecules, and hence, activation of the fluorophore occurs but only within live targeted cells and not in surrounding normal cells that lack the D-galactose receptor (5). Although this approach is highly sensitive for detecting cancer microfoci *in vivo*, the immunogenicity of avidin has been an obstacle to its translation into clinical studies (13, 14).

Recently, a galactosamine-conjugated serum albumin (GmSA) was proposed as a clinically feasible alternative to avidin, in which GmSA-based probe targets the same D-galactose receptor but is nonimmunogenic and has been extensively used in humans. GmSA, in its radiolabeled form, is used to assess hepatic reserve in Japan. GmSA has higher affinity for D-galactose based on its multivalency and its favorable high isoelectric point (7). Herein, we describe the synthesis and implementation of a self-quenching GmSA molecule with multiple rhodamineX ($n \approx 20$; GmSA-20ROX), which is compared with its unquenched version (GmSA-1ROX). We evaluated the ability of GmSA-20ROX to bind cancer cells and compared the fluorescence intensity *in vivo* of GmSA-20ROX with GmSA-1ROX in a mouse model of ovarian cancer peritoneal metastases.

Materials and Methods

Synthesis of GmSA-rhodamineX conjugate

Galactosamine-conjugated bovine serum albumin (GmSA), which contained 23 galactosamine molecules on a single albumin molecule, was purchased from Sigma Chemical. Amido-reactive rhodamineX was purchased from Molecular Probes, Inc. At room temperature, 500 μg (7.0 nmol) of GmSA in 396 μL of Na_2HPO_4 were incubated for 15 min with either 360 nmol (18 μL/20 mmol/L) of rhodamineX-succinimidyl ester in DMSO for GmSA-20ROX or 360 nmol (18 μL/20 mmol/L) for GmSA-20ROX or 14 nmol (0.7 μL/20 mmol/L) for GmSA-1ROX. The mixture was purified with Sephadex G50 (PD-10; GE Healthcare). GmSA-conjugated rhodamineX samples (GmSA-ROX) were used within 6 h after synthesis.

The rhodamineX concentrations were measured by the absorption at 595 nm with a UV-Vis system (8453 Value UV-Bis system, Agilent Technologies) to confirm the number of rhodamineX molecules conjugated with each GmSA molecule. By changing the concentration of the GmSA solution, the number of fluorophore molecules per GmSA was adjusted to be either 1 (GmSA-1ROX) or 20 (GmSA-20ROX).

The protein concentration of GmSA-ROX samples was determined by measuring the absorption at 280 nm with a UV-Vis system (8453 Value UV-Bis system) using GmSA standard solutions of known concentrations (100, 200, and 400 μg/mL). Then, the protein concentration was calculated using the absorbance value corrected by the absorbance of rhodamineX molecule at 280 nm known from the rhodamineX concentration.

Finally, to validate that, the fluorophores were associated with the respective proteins, and both conjugates were analyzed by gel filtration using a high-performance liquid chromatography system equipped with an in-line UV detector (System Gold, Beckman Coulter, Inc.) and fluorescence detector (FP2020, Jasco, Inc.) using a TSK G2000 60-cm column (TOSO Bioscience LLC) with 0.066 mol/L PBS. The UV absorbance profile of GmSA-20ROX at 280 nm was validated to be consistent with the fluorescence profile, which was measured at 610 nm for GmSA-20ROX.

Cell culture

An established ovarian cancer cell line, SHIN3 (15), was used for *in vitro* fluorescence microscopy, flow cytometry, and *in vivo* optical imaging for i.p. disseminated cancer implants. The SHIN3 cells were grown in RPMI 1640 (Life Technologies) containing 10% fetal bovine serum (Life Technologies), 0.03% L-glutamine at 37°C, 100 units/mL penicillin, and 100 μg/mL streptomycin in 5% CO_2.

Transfection of red fluorescent protein (DsRed2) in the SHIN3 cell

The red fluorescent protein (RFP DsRed2)-expressing plasmid was purchased from Clontech Laboratories, Inc. The plasmid was transfected into the SHIN3 cells to validate the results with the targeted fluorophores (see below). The transfection of RFP was done with the electroporation method using Gene Plus II (Bio-Rad Laboratories). Briefly, 3 μg of DsRed2-expressing plasmid were mixed with 2 million SHIN3 cells in 400 μL of the cell culture medium (RPMI 1640 with 10% FCS). Then, the cell suspension was put in a pulse cuvette (Bio-Rad Laboratories) and 250 V pulses were delivered after 950 cycles.

Flow cytometry

One-color flow cytometry was done to compare the fluorescing capabilities of GmSA-1ROX and GmSA-20ROX in SHIN3 cancer cells. SHIN3 cells (5×10^5) were plated on a 12-chamber culture well and incubated for 16 h. GmSA-1ROX or GmSA-20ROX was added to the medium (1 μg/mL), and the cells were incubated for 30 min, 1 h, 3 h, and 6 h. Cells were washed once with PBS and trypsinized and flow cytometry was done. A 488-nm argon ion laser was used for excitation. Signals from cells were collected using a 585/42-nm band-pass filter. Cells were analyzed in a FACScan cytometer (Becton Dickinson) and all data were analyzed using CellQuest software (Becton Dickinson). The fluorescence intensity of each fluorophore was expressed as the mean fluorescence index (MFI). A regression line was calculated from the data sets of incubation time and MFI value and then plotted as a function of incubation time using Microsoft Excel 2003 (Microsoft). The MFI value at each time point and the slope of the regression line were compared between GmSA-1ROX and GmSA-20ROX (7).

Fluorescence microscopy

SHIN3 cells (2×10^4) were plated on a cover glass bottom culture well and incubated for 10 h. GmSA-1ROX or GmSA-20ROX was added to the medium (1 μg/mL) and the cells were incubated for 10 min, 30 min, or 3 h. Cells were washed once with PBS and fluorescence microscopy was done using an Olympus BX51 microscope (Olympus America, Inc.) equipped with the following filters: excitation wavelength, 530 to 570 nm, and emission wavelength, 590 nm long pass. Transmitted light differential interference contrast images were also acquired.

In vitro chemical analysis of activation

Measurement of fluorescence intensity at different acidic conditions. To compare the fluorescing capability of GmSA-1ROX and GmSA-20ROX under different acidic conditions *in vitro*, fluorescence intensity and emission spectra of GmSA-1ROX and GmSA-20ROX were measured with the Maestro In-Vivo Imaging System (CRi, Inc.) in arbitrary units (a.u.). GmSA-1ROX (5 μg) or GmSA-20ROX (5 μg) in 390 μL phosphate buffers with pH 2.3, 3.3, 5.2, 6.4, and 7.4 was put in a nonfluorescent 96-well plate (Costar, Corning, Inc.) and spectral fluorescence imaging was done. A band-pass filter from 503 to 555 nm and a long-pass filter over 580 nm were used for emission and excitation light, respectively. The tunable filter was automatically stepped in 10-nm increments from 500 to 800 nm while the camera captured images at each wavelength interval with constant exposure. Spectral unmixing algorithms were applied to create the unmixed image of the GmSA-1ROX and GmSA-20ROX. A region of interest (ROI) as large as each well was drawn to determine the emission spectra and the fluorescence intensity of two probes using commercial software (Maestro software, CRi). A regression line was calculated from the data sets of pH value and fluorescence intensity on unmixed images and then plotted as a function of pH value using Microsoft Excel 2003.

The fluorescence intensity value at each pH and the slope of the regression line were compared between GmSA-1ROX and GmSA-20ROX (4).

Enzyme activation of fluorescence signal. Enzymatic activation of GmSA-1ROX and GmSA-20ROX by trypsin (Invitrogen), cathepsin C (Sigma-Aldrich, Inc.), cathepsin D (Sigma-Aldrich), and MMP-2 (Sigma-Aldrich) was studied. Trypsin, cathepsin C, cathepsin D, or MMP-2 dissolved in 390 μL phosphate buffers (pH 7.4 for trypsin and MMP-2, pH 6.4 for cathepsin C, and pH 4.5 for cathepsin D) was mixed with 2.5 μg GmSA-1ROX or 2.5 μg GmSA-20ROX. Concentrations of trypsin, cathepsin C, cathepsin D, and/or MMP-2 were 0.05%, 1 unit/mL, 1 unit/mL, and 1 unit/mL, respectively. The mixture was then incubated at 37°C for 0, 1, 3, and 6 h. Spectral fluorescence images were obtained using the Maestro In-Vivo Imaging System and the fluorescence signal was measured using the same method described above. To compare the fluorescence activation of GmSA-1ROX and GmSA-20ROX, the fluorescence intensity immediately after incubation with each enzyme was adjusted to be 1 in a.u. (relative signal intensity). A regression line was calculated from the data sets of relative signal intensity and incubation time and then plotted as a function of incubation time using Microsoft Excel 2003. The slope of the regression line was compared between GmSA-1ROX and GmSA-20ROX. All experiments were done in triplicate.

Detergent activation of fluorescence signal. To evaluate the dequenching ability of GmSA-20ROX, 90 μL of 20% SDS, a detergent, were added to 270 μL/5 μg of either GmSA-20ROX or GmSA-1ROX in PBS at pH 7.4 at room temperature. As control, 90 μL PBS was added to another set of samples. Immediately after mixing the SDS, spectral fluorescence images were obtained using the Maestro In-Vivo Imaging System and the fluorescence signal was measured as the same method as described above. The same experiment was repeated five times.

Additionally, 600 μL/75 μg of either GmSA-20ROX or GmSA-1ROX were placed in the plastic cuvette and excited from the bottom by a 380-nm UV lamp. The 200 μL of 20% SDS were added to each cuvette and mixed well immediately. The entire process of activation was recorded by a digital video camera (Coolpix 5100, Nikon).

Animal model of peritoneal metastases

All procedures were carried out in compliance with the Guide for the Care and Use of Laboratory Animal Resources (1996), National Research Council, and approved by the National Cancer Institute Animal Care and Use Committee. The i.p. tumor xenografts were established by i.p. injection of 2×10^6 SHIN3 or SHIN3 transfected with RFP DsRed2 cells suspended in 200 μL PBS in female nude mice (National Cancer Institute Animal Production Facility, Frederick, MD). Experiments with tumor-bearing mice were done at 14 days after injection of the cells.

In vivo spectral fluorescence imaging

GmSA-1ROX (50 μg) or GmSA-20ROX (50 μg) was diluted in 300 μL PBS and injected into the peritoneal cavities of mice with peritoneally disseminated cancer implants. Each set of two mice (one for each probe) was repeated in triplicate. Immediately, 1 and 3 h after i.p. injection, both mice were sacrificed with carbon dioxide inhalation. Immediately after sacrifice, the abdominal cavity was exposed and both mice were placed side by side on a black plate to compare the fluorescence intensity of the tumors. Spectral fluorescence images were obtained using the Maestro In-Vivo Imaging System. Whole abdominal images, as well as close-up images of the peritoneal membrane, were obtained. A band-pass filter from 503 to 555 nm and a long-pass filter over 580 nm were used for emission and excitation light, respectively. The tunable filter was automatically stepped in 10-nm increments from 500 to 800 nm while the camera captured images at each wavelength interval with constant exposure. The spectral fluorescence images consisting of autofluorescence spectra and the spectra from the probes were obtained and then unmixed based on their spectral patterns using commercial software (Maestro software).

Using the unmixed fluorescence image of the two peritoneal membranes, fluorescence intensity of the cancer implants was semiquantitatively compared between the two probes. A ROI as large as the peritoneal membrane was drawn inside the bowel, and a histogram (number of pixels at specific fluorescence intensity) was created using ImageJ software.[3] Then, a threshold was set in the fluorescence intensity above which a pixel is counted. The total number of pixels (N) within the threshold range was calculated at a threshold value of t (Eq. A).

$$N_{(t)} = \sum_{i=t}^{\infty} n_{(i)} \qquad (A)$$

where i is the fluorescence intensity in a.u., n is the number of pixels at the fluorescence intensity of i, t is the threshold value, and N is the total umber of pixels within the threshold range ($i \geq t$; ref. 4). The common logarithm (log) values of N were calculated and plotted as a function of t. The regression line was calculated from these data sets (t and log$N$) using Microsoft Excel 2003. For comparison of the fluorescent intensity or the "brightness," the slope of regression line was compared between the two fluorophores.

Assessment of the sensitivity and specificity of GmSA-1ROX and GmSA-20ROX for the detection of peritoneal cancer foci

Sensitivity and specificity of GmSA-1ROX and GmSA-20ROX imaging for the detection of peritoneal disseminated cancer foci were studied using three tumor-bearing mice for each probe. The i.p. tumor xenografts were established 14 days after i.p. injection of 2×10^6 RFP-transfected SHIN3 cancer cells suspended in 200 μL PBS in female nude mice (National Cancer Institute Animal Production Facility). Three hours after i.p. injection of 50 μg GmSA-1ROX or 50 μg GmSA-20ROX diluted in 300 μL PBS, spectral fluorescence images of the peritoneal membranes were obtained by Maestro In-Vivo Imaging System. For each mouse, two different parts of the peritoneal membranes were randomly selected and spread out on a black plate and close-up spectral fluorescence imaging was done. ROIs were drawn both within the nodules depicted by RFP spectral unmixed images (standard reference for cancer foci) and in the surrounding adjacent areas (standard reference for noncancerous foci), and the average fluorescence intensity of each ROI was calculated both on the RFP and the GmSA-1ROX or GmSA-20ROX spectral unmixed images using commercial software (Maestro software version 2). The number of ROIs drawn in the noncancerous areas was almost the same as that drawn in the cancer foci. All visible nodules with short-axis diameters of ≥0.8 mm on RFP spectral unmixed images were included for analysis because the minimum possible diameter of a ROI with this software is 0.8 mm. Then, additional ROIs were drawn in the nodules depicted only by the spectral unmixed GmSA-1ROX or GmSA-20ROX images to count the number of false-positive lesions. The average fluorescence intensities of false-positive foci were calculated both on the RFP and the GmSA-1ROX or GmSA-20ROX unmixed images. True positives for GmSA-1ROX or GmSA-20ROX were defined as average fluorescence intensity ≥10 (a.u.), whereas true negatives for GmSA-1ROX or GmSA-20ROX were defined as average fluorescence intensity <10 (a.u.) on the spectral unmixed images. The number of foci positive for both GmSA-1ROX and RFP or GmSA-20ROX and RFP, negative for both GmSA-1ROX and RFP or GmSA-20ROX and RFP, and positive only for GmSA-1ROX or GmSA-20ROX or RFP was counted. Sensitivity of GmSA-1ROX or GmSA-20ROX for the detection of peritoneal cancer foci was defined as the number of peritoneal foci positive for both GmSA-1ROX and RFP or GmSA-20ROX and RFP divided by the number of peritoneal foci positive for RFP. Specificity of GmSA-1ROX or GmSA-20ROX was defined as the number of peritoneal foci negative for both RFP and GmSA-1ROX or RFP and GmSA-20ROX divided by the number of peritoneal foci negative for RFP.

[3] http://rsb.info.nih.gov/ij/plugins/mri-analysis.html

Results

Intracellular activation of GmSA-20ROX reagent

GmSA-20ROX fluoresces more intensely after internalization within cancer cells than GmSA-1ROX. To compare the serial fluorescence intensity of SHIN3 cancer cells, one-color flow cytometry was done at 30 min, 1 h, 3 h, and 6 h after incubation with 1 μg/mL GmSA-1ROX or GmSA-20ROX. GmSA-1ROX showed a small rightward shift during the incubation period of 6 h, whereas GmSA-20ROX showed a significant rightward shift (>1 log shift) compared with SHIN3 control cells at 6 h (Fig. 1A). The MFI for both GmSA-1ROX and GmSA-20ROX consistently increased during the incubation periods of 6 h. MFI values immediately, 30 min, 1 h, 3 h, and 6 h after incubation with GmSA-1ROX were 4.0, 4.0, 4.4, 5.4, and 6.8, respectively, whereas MFI values immediately, 30 min, 1 h, 3 h, and 6 h after incubation with GmSA-20ROX were 4.0, 4.9, 8.0, 24.3, and 35.4, respectively. At 3 h or later after incubation, the fluorescence intensity of SHIN3 cancer cells incubated with GmSA-20ROX became approximately five times higher than that of GmSA-1ROX. Slopes of regression lines, calculated from the MFI and incubation time, were 0.485 a.u./h (r = 0.997) for GmSA-1ROX and 5.574 a.u./h (r = 0.986) for GmSA-20ROX. The results indicate that GmSA-20ROX became more fluorescent (approximately five times) than GmSA-1ROX after internalization into SHIN3 cancer cells.

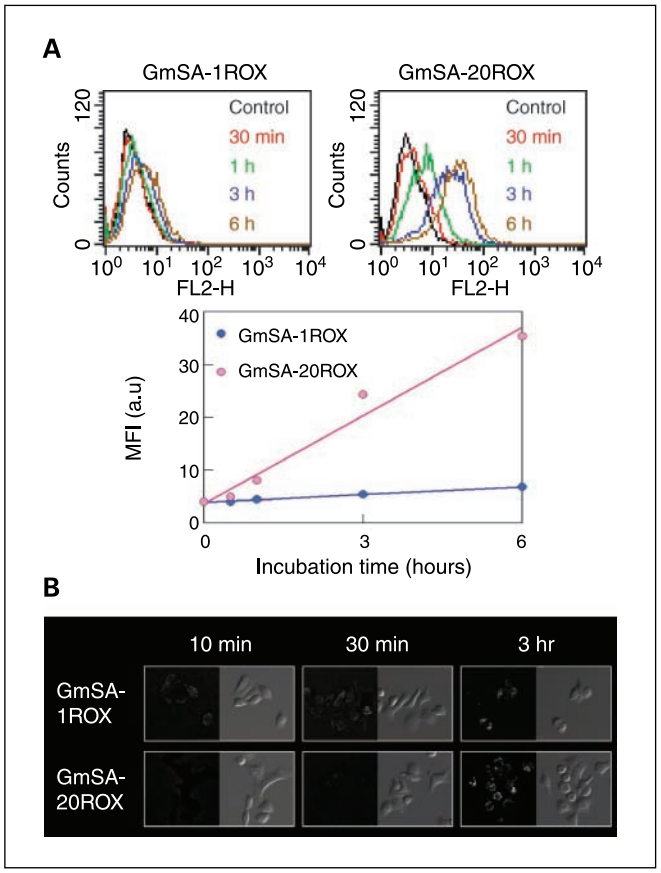

Fig. 1. *A,* serial flow cytometry of SHIN3 cancer cells instilled with GmSA-1ROX or GmSA-20ROX. GmSA-20ROX showed a significant rightward shift (>1 log shift) compared with SHIN3 control cells ≥3 h after incubation (*top right*), whereas GmSA-1ROX failed to show a significant rightward shift (*top left*). The MFI progressively increased in both GmSA-1ROX and GmSA-20ROX. The slopes of regression lines, calculated from MFI and incubation time, were 0.485 a.u./h for GmSA-1ROX and 5.574 a.u./h for GmSA-20ROX, indicating greater fluorescence amplification with GmSA-20ROX compared with GmSA-1ROX. *B,* serial fluorescence microscopy images of SHIN3 ovarian cancer cells. Fluorescent microscopy as well as differential interference contrast imaging were done 10 min, 30 min, and 3 h after incubation with 1 μg/mL of GmSA-1ROX or GmSA-20ROX. The fluorescent dots produced by GmSA-20ROX were initially very small and minimally fluorescent (~30 min) but became much more apparent at 3 h after incubation. Unlike the temporal changes observed in GmSA-20ROX, GmSA-1ROX showed a minimal and gradual change in the size and intensity of intracellular fluorescent dots. Original magnification, × 200. Photographic exposure time: GmSA-1ROX, 1 s; GmSA-20ROX at 10 and 30 min, 1 s; and GmSA-20ROX at 3 h, 100 μs.

GmSA-20ROX becomes markedly fluorescent after entering into endosomes or lysosomes. To investigate the temporal sequence of intracellular fluorescence activation, serial images of SHIN3 ovarian cancer cells incubated with 1 μg/mL of GmSA-1ROX or GmSA-20ROX were obtained with a fluorescence microscopy and differential interference contrast imaging. Fluorescence microscopy initially showed several fine fluorescent dots on the cell surface with minimal cytoplasmic fluorescence at 10 min after incubation with GmSA-1ROX; however, fluorescent dots were barely seen with GmSA-20ROX at the same time point (Fig. 1B). At 30 min after incubation, the number of fluorescent dots increased slightly with GmSA-1ROX and GmSA-20ROX. Three hours later, the number of fluorescent dots produced by GmSA-1ROX increased; however, unlike the gradual increase in light intensity observed with GmSA-1ROX, the size and the intensity of the fluorescent dots produced by GmSA-20ROX dramatically increased at this time (Fig. 1B). These results indicate that, once GmSA-20ROX is bound to the cell surface and internalized, it becomes highly fluorescent due to lysosomal degradation of the complex and resulting dequenching.

In vitro chemical analysis for activation

Signal intensity from both GmSA-20ROX and GmSA-1ROX decreased and their emission peaks shifted toward longer wavelengths under acidic condition. Spectra of GmSA-1ROX at pH 3.3, 5.2, 6.4, and 7.4 contained an emission peak at a wavelength of 610 nm, whereas at pH 2.3 the spectrum contained an emission peak at a wavelength of 620 nm when stepped in 10-nm increments (Fig. 2A). Spectra of GmSA-20ROX at pH 5.2, 6.4, and 7.4 contained an emission peak at a wavelength of 610 nm, whereas at pH 2.3 and 3.3 the spectra contained an emission peak at a wavelength of 620 nm (Fig. 2A). The fluorescence signal intensity of GmSA-1ROX changed little, whereas the intensity of GmSA-20ROX was lower overall and decreased further under highly acidic conditions (Fig. 2A). The fluorescence intensities of GmSA-1ROX at pH 2.3, 3.3, 5.2, 6.4, and 7.4 were 151, 225, 231, 227, and 213 a.u. and those of GmSA-20ROX were 41, 75, 93, 152, and 146 a.u., respectively (Fig. 2A). When the regression lines were calculated as a function of pH values, the slopes of GmSA-1ROX and GmSA-20ROX were 0.023 and 0.105, respectively. These results indicate that the fluorescence intensity of GmSA-1ROX is higher than that of GmSA-20ROX under the same dose and the same acidic conditions, but the fluorescence intensity of GmSA-20ROX is more strongly quenched by acidic conditions.

In vitro ***enzymatic activation of fluorescence was modest and slow in both GmSA-1ROX and GmSA-20ROX.*** Because acidic condition itself could not activate GmSA-1ROX or GmSA-20ROX,

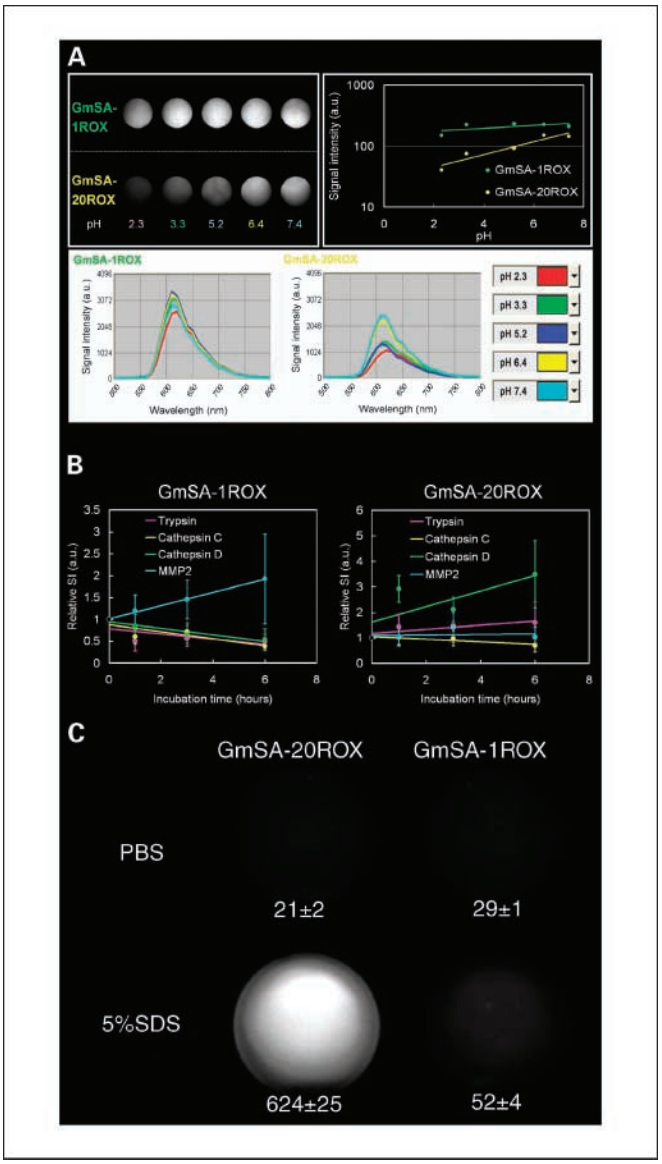

Fig. 2. *A,* optical characteristics of GmSA-1ROX and GmSA-20ROX under acidic conditions. GmSA-1ROX (5 μg) and GmSA-20ROX (5 μg) in 390 μL phosphate buffer (pH 2.3, 3.3, 5.2, 6.4, and 7.4) were placed in a nonfluorescent 96-well plate (*top left*) and spectral fluorescence images were obtained. Emission spectra of GmSA-1ROX (*middle*) and GmSA-20ROX (*bottom*) showed the same emission peak at a wavelength of 610 nm when pH was 7.4, but the emission peak was shifted to a slightly longer wavelength under acidic conditions with both GmSA-1ROX and GmSA-20ROX. Top right, slopes of regression lines as a function of pH values in GmSA-1ROX and RmSA-20ROX were 0.023 and 0.105 (a.u.), respectively. *B,* certain proteases minimally activate the fluorescence of both GmSA-1ROX and GmSA-20ROX *in vitro*. The relative fluorescence signal intensity (*SI*) of GmSA-1ROX at 1, 3, and 6 h after incubation was 0.502 ± 0.219, 0.565 ± 0.174, and 0.491 ± 0.172 for trypsin, 0.608 ± 0.165, 0.723 ± 0.197, and 0.392 ± 0.098 for cathepsin C, 0.848 ± 0.265, 0.655 ± 0.200, and 0.539 ± 0.246 for cathepsin D, and 1.198 ± 0.368, 1.455 ± 0.440, and 1.927 ± 1.028 for MMP-2, respectively. Points, mean; bars, SD. The relative signal intensity of GmSA-20ROX at 1, 3, and 6 h after incubation was 1.448 ± 0.484, 1.483 ± 0.667, and 1.600 ± 0.802 for trypsin, 1.025 ± 0.334, 0.982 ± 0.295, and 0.714 ± 0.256 for cathepsin C, 2.918 ± 0.525, 2.121 ± 0.469, and 3.492 ± 1.322 for cathepsin D, and 1.055 ± 0.443, 1.406 ± 0.589, and 1.036 ± 0.404 for MMP-2, respectively. Slopes of GmSA-1ROX were -0.060, -0.080, -0.074, and 0.151 (a.u./h) for trypsin, cathepsin C, cathepsin D, and MMP-2, respectively. Slopes of GmSA-20ROX were 0.079, -0.050, 0.305, and 0.012 (a.u./h) for trypsin, cathepsin C, cathepsin D, and MMP-2, respectively. *C,* activation of GmSA-20ROX by SDS was 16-fold greater than that of GmSA-1ROX. The fluorescence signal of GmSA-20ROX (*left column*) was activated 30-fold [from 21 ± 2 (a.u.) to 624 ± 25 (a.u.)] by the addition of 5% SDS. In contrast, GmSA-1ROX (*right column*) was activated only 1.8-fold [from 29 ± 1 (a.u.) to 52 ± 4 (a.u.)] by the addition of 5% SDS.

enzymatic activation of GmSA-1ROX or GmSA-20ROX was studied using trypsin, cathepsin C, cathepsin D, and MMP-2. The slopes of regression lines calculated from the data sets of serial relative fluorescent signal intensity of GmSA-1ROX and the incubation time were -0.060, -0.080, -0.074, and 0.151 (a.u./h) for trypsin, cathepsin C, cathepsin D, and MMP-2, respectively (Fig. 2B). For GmSA-20ROX, the slopes of trypsin, cathepsin C, cathepsin D, and MMP-2 were 0.079, -0.050, 0.305, and 0.012 (a.u./h), respectively (Fig. 2B). With respect to the current incubation protocols, only MMP-2 activated the fluorescence of GmSA-1ROX, whereas trypsin, cathepsin D, and MMP-2 activated the fluorescence of GmSA-20ROX, with cathepsin D producing the strongest gain in fluorescence.

SDS can activate the fluorescence signal of GmSA-20ROX 16-fold greater than that of GmSA-1ROX. Because enzymatic activation of GmSA-1ROX or GmSA-20ROX was slow and limited compared with the observed activation of GmSA-20ROX in SHIN3 cells, activation was induced by adding a detergent, SDS. SDS (5%) activated GmSA-20ROX signal from 21 (a.u.) to 624 (a.u.), whereas GmSA-1ROX was activated from 29 (a.u.) to 52 (a.u.; Fig. 2C). The activation happened immediately after mixing SDS with samples and was stable at least for 30 min.

This quick and intense activation of GmSA-20ROX with addition of SDS can be captured by video (Supportive video 1) and is most similar to the activation observed after the intracellular activation of GmSA-20ROX as shown in Fig. 1.

In vivo imaging of peritoneal metastasis with activatable GmSA-20ROX probe

GmSA-20ROX produces higher target to background fluorescence within tumor nodules* in vivo *than GmSA-1ROX. Immediately after i.p. injection with GmSA-1ROX or GmSA-20ROX, the fluorescence intensity of GmSA-20ROX was comparable with that of GmSA-1ROX, but tumor nodules were hard to detect due to free complex in the peritoneal cavity (Fig. 3A). By 1 h after i.p. injection, the fluorescence intensity arising from tumor nodules using GmSA-20ROX was higher than GmSA-1ROX and the background signal was comparable. By 3 h after injection, the fluorescence intensity of the tumor nodules was visually higher with GmSA-20ROX than with GmSA-1ROX (Fig. 3A). Although a small amount of fluorescence was noted from biliary excretion after i.p. injection with GmSA-20ROX due to transperitoneal systemic absorption, the peritumoral background signal was comparable between the two groups. Submillimeter cancer foci were clearly visualized by close-up imaging of the peritoneal membranes (Fig. 3A).

To make an objective comparison of fluorescence intensity generated by GmSA-1ROX and GmSA-20ROX, ROI measurements were drawn on peritoneal surfaces using the unmixed fluorescence image and a histogram depicting the distribution of pixel intensities was created (Fig. 3B). The dynamic range of signal intensity in the unmixed fluorescence image was set from 1 to 256 in a.u. and the threshold value (t) was changed from 31 to 241 in increments of 10 because the background signals, such as the normal peritoneal membrane excluding tumors and the black plate, were mostly <31 (a.u.). Then, the total number of pixels (N) within the threshold range was calculated as a function of threshold (t) and a regression line was calculated in each ROI (Fig. 3B). The correlation coefficients of GmSA-1ROX

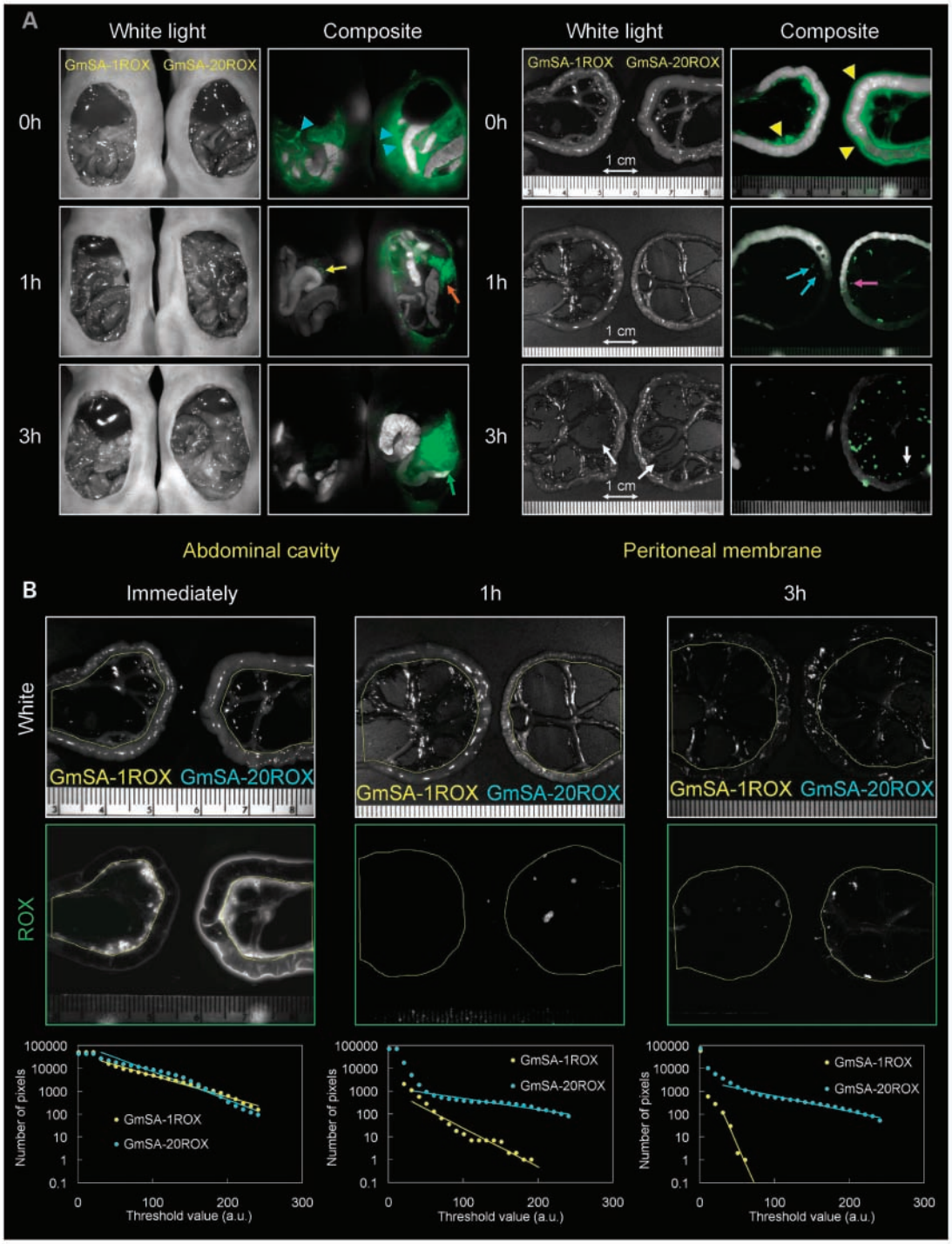

Fig. 3. Serial side-by-side *in vivo* spectral fluorescence images of peritoneally disseminated cancer model after injection with 50 μg GmSA-1ROX or 50 μg GmSA-20ROX. *A,* white light and composite image of the peritoneal cavity and the peritoneal membrane. Immediately after injection, aggregated tumor foci (abdominal cavity) and disseminated cancer implants (peritoneal membrane) were undetectable due to high background signals (*blue* and *yellow arrowheads*, respectively). At 1 h after injection, GmSA-20ROX clearly depicted the aggregated tumor foci (*red arrow*) and the submillimeter peritoneal implants (*pink arrow*), whereas GmSA-1ROX minimally visualized the cancer foci (*yellow* and *blue arrows*) due to the insufficient fluorescence intensity from the cancer cells. At 3 h after injection, aggregated tumor foci as well as submillimeter peritoneal implants were more clearly visualized by GmSA-20ROX, whereas GmSA-1ROX failed to show the cancer foci due to insufficient fluorescence, although small cancer foci were detected by white light images. *B,* semiquantitative assessment of *in vivo* fluorescence intensities of GmSA-1ROX and GmSA-20ROX. ROI was drawn i nside the intestine on the unmixed GmSA-ROX fluorescence image using both the white light (*top*) and unmixed rhodamineX image (*middle*). Histogram of fluorescence intensity of a ROI drawn on each of the peritoneal membranes instilled with GmSA-1ROX and GmSA-20ROX. The dynamic range of the fluorescence intensity was split into equal-sized 256 bins (1 – 256). Then, for each bin (*X axis*), the number of pixels from the data set that fall into each bin (*Y axis*) is counted. The regression lines were calculated from the data sets (fluorescence threshold values 31 – 241, total number of pixels within the threshold range 1 – 100,000 in common logarithm). Bottom, the slopes of GmSA-1ROX and GmSA-20ROX were -0.009 and -0.012 for immediate, -0.017 and -0.005 for 1 h, and -0.074 and -0.007 for 3 h after injection, respectively.

and GmSA-20ROX were -0.990 and -0.978 for immediately after injection, -0.968 and -0.950 for 1 h after injection, and -0.946 and -0.988 for 3 h after injection, respectively. The slopes of GmSA-1ROX and GmSA-20ROX were -0.009 and -0.012 immediately after injection, -0.017 and -0.005 at 1 h after injection, and -0.074 and -0.007 at 3 h after injection, respectively. These results indicate that the fluorescence of GmSA-1ROX decreased over time, whereas that of GmSA-20ROX was either maintained or activated during the incubation time of 3 h.

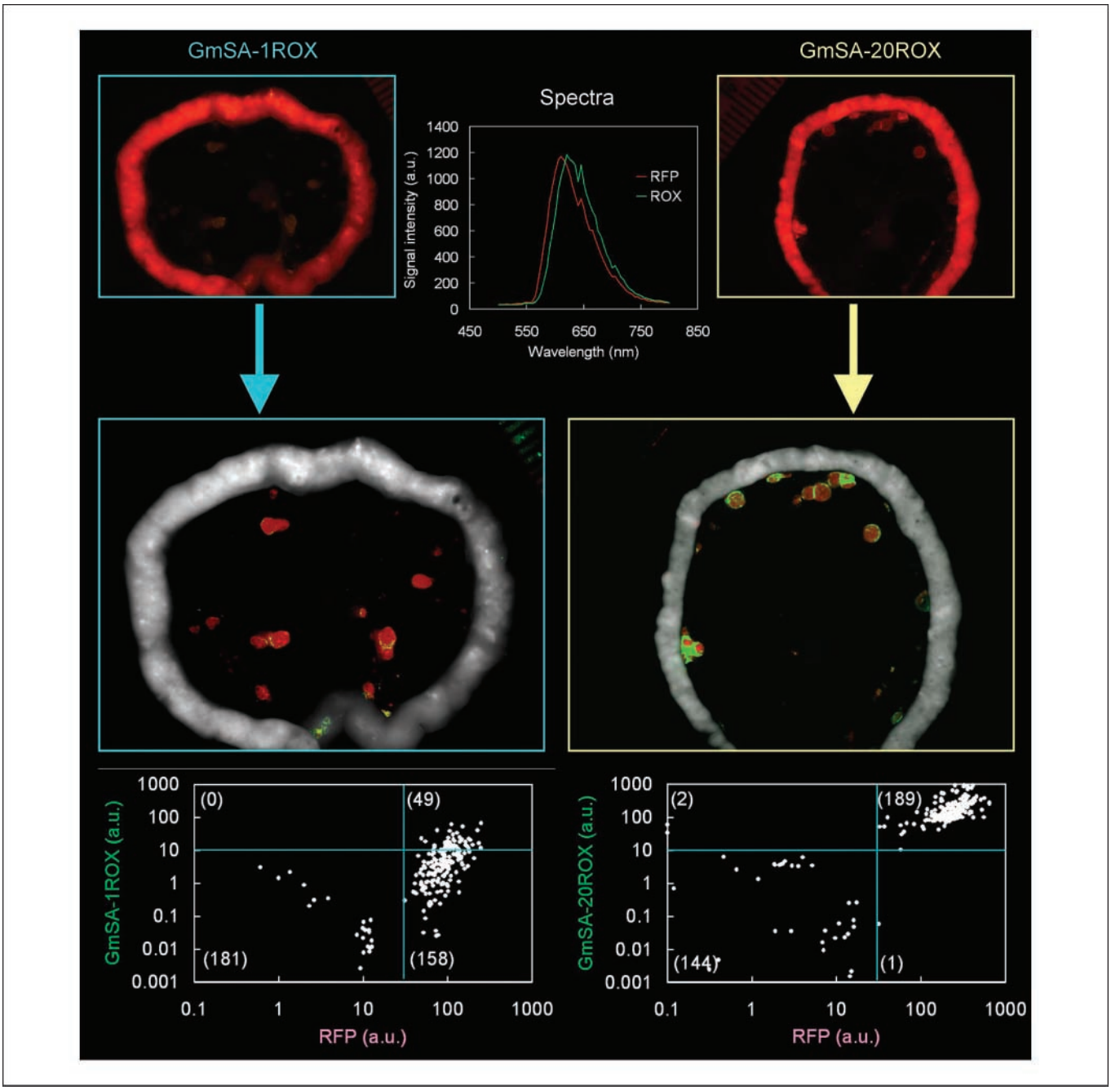

Fig. 4. Sensitivity of GmSA-20ROX spectral fluorescence imaging to detect peritoneal cancer foci was higher than that of GmSA-1ROX. *In vivo* spectral fluorescence imaging of RFP-transfected SHIN3 ovarian cancer – bearing peritoneal membrane was done 3 h after injection with 50 μg GmSA-1ROX or 50 μg GmSA-20ROX. The spectral fluorescence image was unmixed based on the spectral patterns (*top middle*) of GmSA-1ROX and GmSA20ROX, as well as the autofluorescence, and then, composite images consisting of GmSA-ROX (*green*), RFP (*red*), and autofluorescence (*black* and *white*) were made. Most foci detected by unmixed GmSA-1ROX images or GmSA-20ROX images were colocalized with unmixed RFP images. Two-color *in vivo* fluorescence intensity plots of the foci detected by unmixed GmSA-ROX images, unmixed RFP images, or both and nontumorous areas (*bottom left*, GmSA-1ROX; *bottom right*, GmSA-20ROX). All foci with signal intensities ≥30 (a.u.) on spectral unmixed RFP images and diameters ≥0.8 mm were defined as cancer foci (n = 207 for GmSA-1ROX and n = 190 for GmSA-20ROX). For comparison, ROIs were drawn in the surrounding nontumorous areas on the unmixed RFP images. When the foci positive for GmSA-ROX were defined as those whose fluorescence intensities ≥10 (a.u.) on spectral unmixed GmSA-1ROX images or GmSA-20ROX images, sensitivity and specificity were 24% (49 of 207) and 100% (181 of 181) for GmSA-1ROX and 99% (189 of 190) and 99% (144 of 146) for GmSA-20ROX, respectively.

Sensitivity of GmSA-20ROX for the detection of RFP-labeled cancer foci was superior to GmSA-1ROX. Sensitivity and specificity of spectrally unmixed imaging to detect peritoneal cancer foci were compared between GmSA-1ROX and GmSA-20ROX using RFP-transfected SHIN3 cancer cells. Both unmixed GmSA-1ROX and GmSA-20ROX images showed ring-like accumulation around the cancer foci, which were depicted by the unmixed RFP images (Fig. 4). RFP-positive foci (positive standard) were defined as those whose fluorescence intensities were ≥30 (a.u.) on unmixed RFP images, and GmSA-ROX–positive foci were defined as those whose fluorescence intensities were ≥10 (a.u.) on unmixed GmSA-1ROX images or GmSA-20ROX images. Forty-nine foci showed GmSA-1ROX fluorescence intensities ≥10 (a.u.) among the 207 RFP-positive foci >0.8 mm in diameter (Fig. 4). One hundred eighty-one foci showed GmSA-1ROX fluorescence intensities <10 (a.u.) among the 181 RFP-negative foci [i.e., fluorescence intensities <30 (a.u.) on unmixed RFP images]. Thus, the spectral unmixed GmSA-1ROX image had a sensitivity of 24% (49 of 207) and a specificity of 100% (181 of 181). In contrast, unmixed GmSA-20ROX images showed that 189 foci showed GmSA-20ROX fluorescence intensities ≥10 (a.u.) among the 190 RFP-positive foci (Fig. 4). One hundred forty-four foci showed GmSA-20ROX fluorescence intensities <10 (a.u.) among the 146 RFP-negative foci. Thus, the spectrally unmixed GmSA-20ROX imaging had a sensitivity of 99% (189 of 190) and a specificity of 99% (144 of 146).

Discussion

Although ovarian cancer implants can be targeted using an avidin-3 rhodamineX complex, there are several reasons to consider alternative complexes. GmSA-20ROX is substantially less immunogenic compared with avidin, and GmSA has been used as the basis for a technetium-99m–labeled radiopharmaceutical to assess hepatic reserve in humans. Additionally, GmSA-20ROX binds target cells more rapidly and more efficiently than avidin due to its multivalency (7, 16). Because GmSA synthesis involves the conjugation of 23 D-galactosamines reacted with carboxyl groups rather than amino groups on an albumin molecule (7), there are multiple binding sites for the D-galactose receptor and the molecule has a favorably high isoelectric point (7, 16). Moreover, activation via dequenching of the rhodamineX after cellular internalization provides a generalizable platform for targeted fluorescent probes by exchanging the targeting moiety (5). We used the D-galactose receptor as a target in this study because it is expressed in a wide range of cancers, which metastasize i.p. (6). Finally, compared with other mechanisms of activation, GmSA seems to activate rapidly by unfolding the linear protein chain and produces intense fluorescence signal via dequenching. In contrast, proteolytic activation (e.g., trypsin, cathepsin C, and cathepsin D) requires more time for digestion (Fig. 2C). The protease generally takes a longer time to completely digest target compound (9, 10). In the case of avidin-3 rhodamineX tetramer, dissociation into monomers is a physical reaction that can quickly induce the efficient dequenching of avidin-3 rhodamineX (5). Unfolding is a common response of proteins once in the acidsome and is used by cells to efficiently digest and recycle the protein by acid proteases, such as cathepsin C and cathepsin D. In theory, unfolding cannot induce dequenching as efficiently as dissociation. In reality, protein unfolding can lead to rapid activation of quenched fluorophores, GmSA-20ROX (30-fold overall; 1.5-fold/rhodamineX), which is not as efficient as avidin-3 rhodamineX (40-fold; 13-fold/rhodamineX). Because GmSA is a very hydrophilic protein due to the large number of conjugated sugar molecules, up to 20 rhodamineX molecules can be loaded on a single GmSA molecule. Thus, GmSA-20ROX is rapidly activated once it is internalized within cancer cells and enters the lysosomes where the GmSA molecules are both unfolded and digested.

Although the original fluorescence intensity of GmSA-20ROX was almost two thirds of GmSA-1ROX in PBS, GmSA-20ROX images immediately after i.p. injection were unsatisfactory compared with GmSA-1ROX (Fig. 1). Background signals of GmSA-20ROX were higher, resulting in limited target-to-background ratios (Fig. 3A). One of the reasons is that ascites or serum can also partially activate the fluorescence of GmSA-20ROX (Supplementary Fig. S1). Although the explanation for this phenomenon is unclear, it may be due to an energy transfer from nonfluorescent dimers to excited monomers of the dye due to incomplete unfolding of GmSA-20ROX related to the high protein concentration (5, 17).

The strategy of signal activation by selective binding, internalization, and catabolism and/or metabolism leading to dequenching can be applied to a wide variety of targets on the surface of cancer cells (5, 6). Although we studied the D-galactose receptor on SHIN3 ovarian cancer cells using GmSA, similar unfolding activation strategies could be used with other hydrophilic protein ligands (7). Therefore, by changing the targeting moiety, this strategy can be widely applied to other targets or receptors that are expressed on cancer cells.

We foresee that GmSA-20ROX could be readily used in the operating room by surgeons during cytoreductive surgery for ovarian cancer. Because rhodamineX emits in the visible range of light, surgeons will be able to detect fluorescence from small metastatic ovarian cancer nodules using only glasses fitted with appropriate filters and green excitation light. In the event that this is insufficient for detecting all lesions, it is also possible to augment the detected signal using a fluorescence charge-coupled device camera equipped with specific filters, which would display images in real time during the surgery. Using either approach, the specific fluorescence signal from the target tumors could be used to identify small foci of cancer within the peritoneal cavity and reveal local residual disease that would otherwise escape attention.

In conclusion, a newly synthesized target-specific activatable probe GmSA-20ROX was able to identify tiny foci of peritoneal metastases by binding to D-galactose receptors on the surface membrane of ovarian cancer cells. Within 1 h of incubation with GmSA-20ROX, the agent was internalized into cancer cells and produced high intensity fluorescence. Using a RFP counterstain, GmSA-20ROX showed a 99% sensitivity for peritoneal metastases 0.8 mm or greater in size and had a 99% specificity. This agent may be useful in improving the tumor resection in clinical trials of patients with peritoneal metastases who are undergoing cytoreductive surgery.

References

1. Hama Y, Urano Y, Koyama Y, et al. *In vivo* spectral fluorescence imaging of submillimeter peritoneal cancer implants using a lectin-targeted optical agent. Neoplasia 2006;8:607–12.
2. Achilefu S, Dorshow RB, Bugaj JE, Rajagopalan R. Novel receptor-targeted fluorescent contrast agents for *in vivo* tumor imaging. Invest Radiol 2000;35:479–85.
3. Moon WK, Lin Y, O'Loughlin T, et al. Enhanced tumor detection using a folate receptor-targeted near-infrared fluorochrome conjugate. Bioconjug Chem 2003;14:539–45.
4. Hama Y, Urano Y, Koyama Y, Bernardo M, Choyke PL, Kobayashi H. A comparison of the emission efficiency of four common green fluorescence dyes after internalization into cancer cells. Bioconjug Chem 2006; 17:1426–31.
5. Hama Y, Urano Y, Koyama Y, et al. A target cell-specific activatable fluorescence probe for *in vivo* molecular imaging of cancer based on a self-quenched avidin-rhodamine conjugate. Cancer Res 2007;67:2791–9.
6. Hama Y, Urano Y, Koyama Y, Choyke PL, Kobayashi H. Targeted optical imaging of cancer cells using lectin-binding BODIPY conjugated avidin. Biochem Biophys Res Commun 2006;348:807–13.
7. Hama Y, Urano Y, Koyama Y, Choyke PL, Kobayashi H. D-galactose receptor-targeted *in vivo* spectral fluorescence imaging of peritoneal metastasis using galactosamine-conjugated serum albumin-rhodamine green. J Biomed Opt 2007;12:050501.
8. Kamiya M, Kobayashi H, Hama Y, et al. An enzymatically activated fluorescence probe for targeted tumor imaging. J Am Chem Soc 2007;129:3918–29.
9. Weissleder R, Tung CH, Mahmood U, Bogdanov A, Jr. *In vivo* imaging of tumors with protease-activated near-infrared fluorescent probes. Nat Biotechnol 1999;17:375–8.
10. Tung CH, Mahmood U, Bredow S, Weissleder R. *In vivo* imaging of proteolytic enzyme activity using a novel molecular reporter. Cancer Res 2000;60: 4953–8.
11. Bogdanov AA, Jr., Lin CP, Simonova M, Matuszewski L, Weissleder R. Cellular activation of the self-quenched fluorescent reporter probe in tumor microenvironment. Neoplasia 2002;4:228–36.
12. Hajitou A, Trepel M, Lilley CE, et al. A hybrid vector for ligand-directed tumor targeting and molecular imaging. Cell 2006;125:385–98.
13. Paganelli G, Chinol M, Maggiolo M, et al. The three-step pretargeting approach reduces the human anti-mouse antibody response in patients submitted to radioimmunoscintigraphy and radioimmunotherapy. Eur J Nucl Med 1997;24:350–1.
14. Hytonen VP, Laitinen OH, Grapputo A, et al. Characterization of poultry egg-white avidins and their potential as a tool in pretargeting cancer treatment. Biochem J 2003;372:219–25.
15. Imai S, Kiyozuka Y, Maeda H, Noda T, Hosick HL. Establishment and characterization of a human ovarian serous cystadenocarcinoma cell line that produces the tumor markers CA-125 and tissue polypeptide antigen. Oncology 1990;47:177–84.
16. Tweedle M. Adventures in multivalency. Contrast Media Mol Imaging 2006;1:2–9.
17. MacDonald RI. Characteristics of self-quenching of the fluorescence of lipid-conjugated rhodamine in membranes. J Biol Chem 1990;265:13533–9.

Clinical Cancer Research

A Self-Quenched Galactosamine-Serum Albumin-RhodamineX Conjugate: A "Smart" Fluorescent Molecular Imaging Probe Synthesized with Clinically Applicable Material for Detecting Peritoneal Ovarian Cancer Metastases

Yukihiro Hama, Yasuteru Urano, Yoshinori Koyama, et al.

Clin Cancer Res 2007;13:6335-6343.